Article

Microwave Dielectric Properties of Li₃TiO₃F Oxyfluorides Ceramics

Guoguang Yao [1], Jiuyan Zhao [1], Ya Lu [1], Hongkai Liu [1], Cuijin Pei [1,*], Qian Ding [1], Miao Chen [1], Yaming Zhang [1], Ding Li [1] and Fu Wang [2,*]

[1] School of Science, Xi'an University of Posts and Telecommunications, Xi'an 710121, China
[2] State Key Laboratory of Military Stomatology & National Clinical Research Center for Oral Diseases, Department of Prosthodontics, School of Stomatology, The Fourth Military Medical University, Xi'an 710032, China
* Correspondence: physicas@163.com (C.P.); wangfu99@fmmu.edu.cn (F.W.)

Abstract: Using a solid-state reaction strategy, nominal Li₃TiO₃F oxyfluorides ceramics were fabricated, and its sintering behavior, microstructure, phase assemblages, as well as microwave dielectric performances were all investigated. The main phase of Li₃TiO₃F with cubic structures accompanied with small amounts of the LiF or Li₂TiO₃ secondary phase was identified by XRD analysis. SEM analysis showed that a uniform and dense microstructure was obtained for 750 °C-sintered samples. The dielectric constant (ε_r) and quality factor ($Q \times f$) were found to be strongly correlated with porosity and grain size distribution, whereas the temperature coefficient of resonance frequency (τ_f) was mainly dominated by the phase assemblages. In particular, the 750 °C-sintered Li₃TiO₃F samples exhibited good microwave dielectric performances: ε_r = 18, $Q \times f$ = 57,300 GHz (under 9.2 GHz), τ_f = −43.0 ppm/°C.

Keywords: microwave dielectric performances; ceramics; Li₃TiO₃F; oxyfluorides

1. Introduction

Microwave dielectrics ceramics (MDCs) have become extraordinarily alive with the advent of the fifth-generation (5G) mobile network and the Internet of Things (IoT), which have been widely utilized in miscellaneous microwave devices [1,2]. Among the MDCs, low temperature co-fired ceramics (LTCCs) are able to simultaneously hold low firing temperatures (≤960 °C), moderate permittivity (ε_r), and possess a high quality factor ($Q \times f$), as well as approaching a zero temperature coefficient of resonant frequency (τ_f), which is profitable for the assembling of electronic devices and environmental protection [3,4]. Thus, it is necessary to explore these MDCs, especially the LTCCs, to better meet the current demands for the IoT and 5G era [5–9].

Recently, a series of oxyfluorides have been prepared either by solid solution or anion substitution, which exhibited inherently low sintering temperatures and excellent microwave dielectric performances concurrently [10–12]. For example, in 2019 the structure and microwave dielectric performances of novel Ti-containing oxyfluorides, such as Li₇Ti₃O₉F and Li₅Ti₂O₆F were first reported by Fang et al. [10,11]. Subsequently, several binary, ternary, and multicomponent Nb-containing oxyfluorides with promising microwave dielectric performances, such as Li₅.₅Nb₁.₅O₆F, Li₄Mg₂NbO₆F, and Li₇(Nb₁₋ₓTiₓ)₂O₈₋ₓF, Li₆MgTiNb₁₋ₓVₓO₈F, have been reported by Liu et al. [13–15]. In 2023, Zhang et al. reported a new oxyfluoride dielectric ceramic system of Li₂₊ₓZrO₃Fₓ, among which the Li₃ZrO₃F ceramics simultaneously exhibited a near zero τ_f (1.2 ppm/°C), a high $Q \times f$ (65,100 GHz), and a low firing temperature (925 °C) [16]. The abovementioned research opened a scheme to develop novel LTCCs with superior dielectric performances [16]. Li-containing rock salt structured Li₂AO₃ (A = Ti, Sn, Zr) system ceramics have drawn a tremendous amount of attention due to their promising microwave dielectric performances

(ε_r = 13~22, τ_f = 20~38 ppm/°C and $Q \times f$ = 38,000~120,000 GHz) [17,18]. However, the high heating temperature ($\geq$1300 °C) and non-near zero τ_f have severely impeded the commercial application of Li_2AO_3 ceramics. Through a mixture of Li_2TiO_3 and LiF, along with subsequent sintering, the Li_3TiO_3F major phase has been synthesized by Szymanski and Bian et al. [19,20]. However, the $Q \times f$ (~30,000 GHz) of nominal Li_3TiO_3F ceramics is not high due to the appearance of the LiF second phase. Until now, there are no relative reports on pure phase Li_3TiO_3F ceramics along with their microwave dielectric properties. Thus, in this study, we aimed to fabricate a pure Li_3TiO_3F compound using a solid-state reaction route, and its sinterability, phase assemblages, microstructures and microwave dielectric performances were all further investigated.

2. Materials and Methods

Li_3TiO_3F oxyfluorides were synthesized following a solid-state reaction route. According to the stoichiometric formula of Li_3TiO_3F, the raw materials of Li_2CO_3 (98%, Guo-Yao Co. Ltd., Shanghai, China), LiF (98%, Guo-Yao Co. Ltd., Shanghai, China), and TiO_2 (99.9%, Guo-Yao Co., Ltd., Shanghai, China) were individually weighed, and then milled for 8 h using a planetary ball mill with a milling rate of 350 r/min. After drying, these powders were calcined under 600 °C for 4 h. The prebaked powders were reground after crushing, granulated with 6 wt.% solution of polyvinyl alcohol, and then pressed into cylindrical discs (12 mm-diameter and 6 mm-thick) at 100 MPa. Finally, these cylindrical discs were agglutinated under 500 °C for 2 h to remove the binder, and then fired at 700–800 °C for 5 h. In order to compensate for the volatilization of Li and F during sintering, the samples were muffled with sacrificial powders owing the same composition and in a covered crucible.

The crystalline phases were characterized by X-ray diffraction (XRD, Smartlab, Japan) with CuK_α radiation. XRD data for Rietveld refinement were collected in the range of $10-80°$, with a step size of $0.02°$, and a count time of 1 s. The lattice parameters, phase quantity, and theoretical density of the sample were refined and calculated via GSAS software and Equation (1) (shown below) [21,22]. In Equation (1), % and ρ_m represent the weight percentage and the theoretical density of the given phase, respectively. The bulk densities of the Li_3TiO_3F ceramics were assessed by Archimedes' principle. The microstructures were observed with scanning electron microscopy (SEM, JSM-6610, Jeol, Tokyo, Japan). Using the Rohde & Schwarz network analyzer, the Hakki-Coleman dielectric resonator approach modified by Courtney [23,24] was utilized to measure the microwave dielectric performances of the Li_3TiO_3F ceramics. The τ_f was achieved by Equation (2):

$$\rho_t = \frac{100}{\frac{\%\text{phase1}}{\rho_m\text{phase1}} + \frac{\%\text{phase2}}{\rho_m\text{phase2}}} \tag{1}$$

$$\tau_f = \frac{f_{85} - f_{25}}{f_{25} \times (85 - 25)} \times 10^6 (\text{ppm/°C}) \tag{2}$$

where f_{25} and f_{85} represent the resonant frequency at 25 °C and 85 °C, respectively.

3. Results and Analysis

The bulk density (ρ_b) and relative density (ρ_r) of the Li_3TiO_3F ceramics are illustrated in Figure 1. The theoretical density of sample was gauged from the refined XRD data, as shown in Table 1. Following the rise in heating temperature from 700 °C to 750 °C, the ρ_b and ρ_r of Li_3TiO_3F sintered bodies were found to have enhanced from 2.870 g/cm^3 to 3.150 g/cm^3, and from 89.1% to 98.3%, respectively. The increase in ρ_r resulted from the removal of the porosity, whereas the abatement in ρ_r was due to the over-sintering [25]. From the view of density, the optimal sintering temperature of the Li_3TiO_3F ceramics was 750 °C. Compared to Li_2TiO_3 ceramics (1300 °C), the inherently low sintering temperature of the Li_3TiO_3F ceramics (750 °C) is benefited from the alleviation of the chemical potential caused by the co-occupied anion position of the F^- and O^{2-} ions, and a similar phenomenon was reported in our previous article [26].
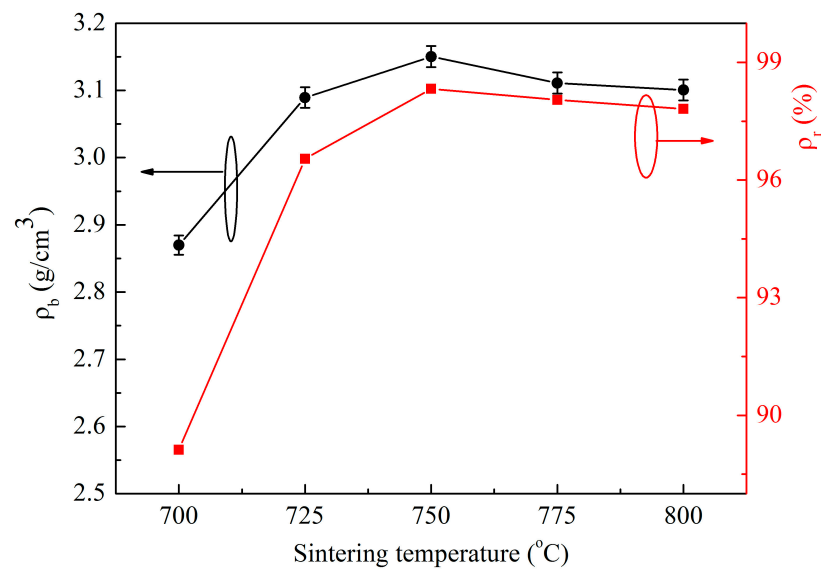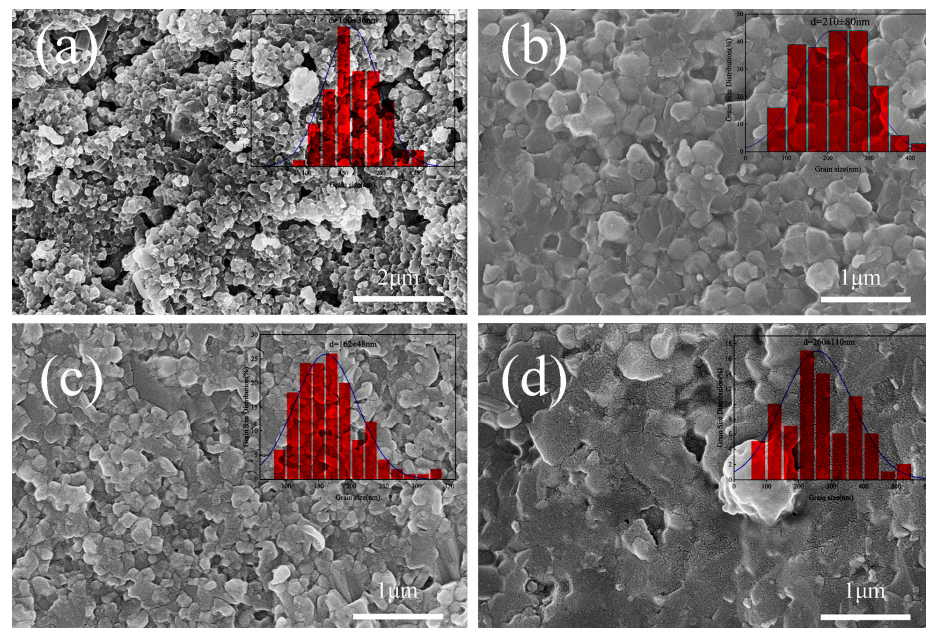
Figure 1. Bulk density (ρ_b) and relative density (ρ_r) of nominal Li_3TiO_3F ceramics sintered at different temperatures.

Table 1. Refinement data of nominal Li_3TiO_3F ceramics sintered under different conditions.

| S.T.	Phase	Phase Quantity	ρ_m	ρ_t	a = b = c	V	Rwp	Rp
(°C)		(%)	(g/cm^{-3})	(g/cm^{-3})	(Å)	(Å^3)	(%)	(%)
725	Li_3TiO_3F	96.657	3.192	3.200	4.133	70.599	8.490	6.720
	Li_2TiO_3	3.343	3.430		8.277	566.980		
750	Li_3TiO_3F	97.245	3.199	3.204	4.130	70.450	9.660	7.420
	Li_2TiO_3	2.755	3.407		8.295	570.830		
775	Li_3TiO_3F	92.367	3.229	3.172	4.126	70.218	8.400	6.620
	LiF	7.633	2.622		4.035	65.707		
800	Li_3TiO_3F	94.102	3.210	3.170	4.125	70.198	7.240	5.780
	LiF	5.898	2.637		4.028	65.337		

Figure 2 displays the typical fresh fracture of nominal Li_3TiO_3F ceramics sintered at different temperatures. Several intergranular pores were observed for the 725 °C-sintered sample. The 750 °C-sintered sample exhibited a relatively uniform and compact microstructure with a mean grain size of around 210 nm, as shown in Figure 2b, corresponding to the achieved maximum relative density. However, when the sintering temperature surpassed 775 °C, poor grain uniformity and exaggerated grain growth appeared as shown in Figure 2c,d, which would therefore deteriorate the sample's dielectric properties.

Figure 3 exhibits the XRD profiles of nominal Li_3TiO_3F specimens fired at 725~800 °C. For the samples sintered at 725 and 750 °C, their XRD patterns were identified as cubic structure Li_3TiO_3F (#04-002-4527) and Li_2TiO_3 (#01-075-1602) phases, and no diffraction peaks of LiF were observed. With increasing the temperature to 775 and 800 °C, except for the major phase Li_3TiO_3F, the diffraction peaks from the Li_2TiO_3 phase vanished, whereas the diffraction peaks from the LiF phase (#01-089-3610) appeared. In our experiment, pure phase Li_3TiO_3F was not obtained, and this was similar with the report published by Bian et al. [20], but somewhat different with the previous report by Szymanski et al. [19].

Figure 2. The typical fresh fracture of nominal Li_3TiO_3F ceramics sintered at different temperatures: (**a**) 725 °C, (**b**) 750 °C, (**c**) 775 °C, and (**d**) 800 °C, respectively.
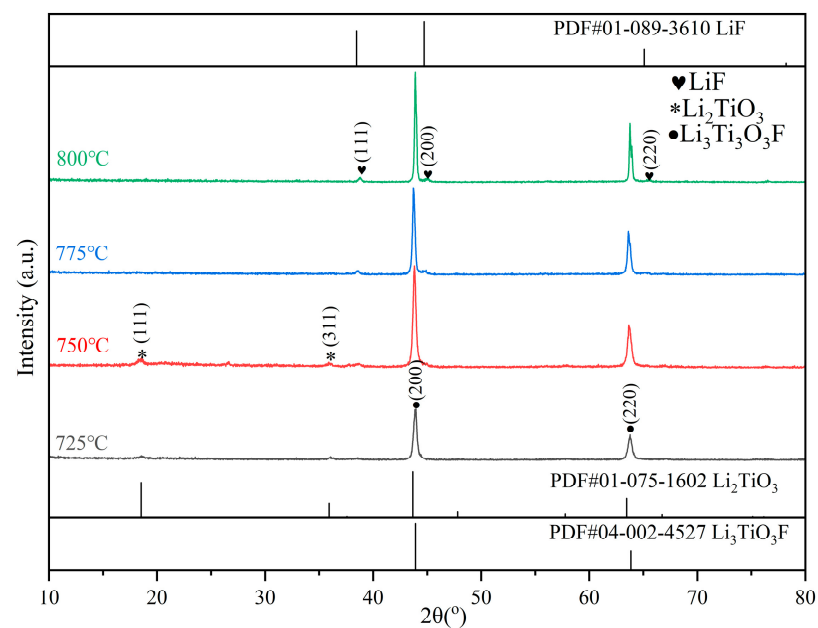

Figure 3. XRD profiles of nominal Li_3TiO_3F specimens fired at 725~800 °C.

To further clarify the crystal structure information and phase assemblage, Rietveld refinements of the XRD data were conducted on the nominal Li_3TiO_3F ceramics via GSAS software using three phase models consisting of Li_3TiO_3F, LiF, and Li_2TiO_3. Figure 4 displays the comparison of the simulated and measured XRD profiles of Li_3TiO_3F specimens fired at 725~800 °C, and the resultant refined results are summarized in Table 1. As shown in Figure 4 and Table 1, small reliability factors below 10% were observed, suggesting that the refinement results obtained were creditable.
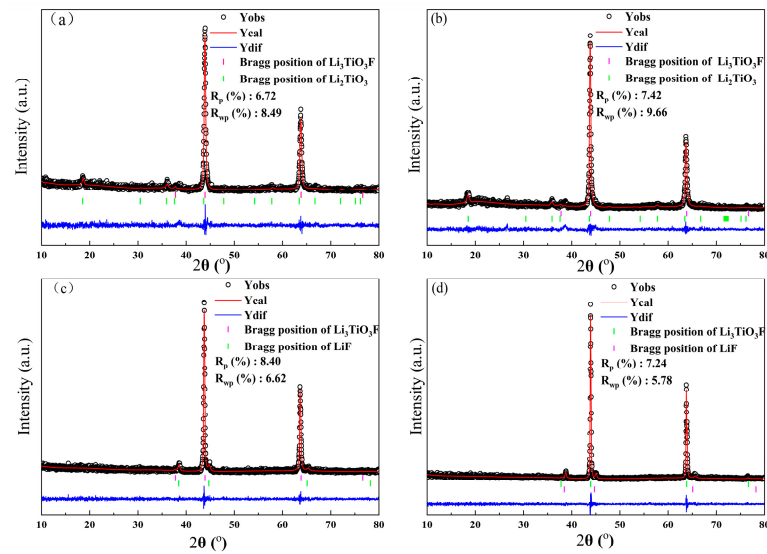
Figure 4. The simulated and measured XRD profiles of nominal Li_3TiO_3F specimens fired at different temperatures: (**a**) 725 °C, (**b**) 750 °C, (**c**) 775 °C, and (**d**) 800 °C.

Figure 5 displays the ε_r values of nominal Li_3TiO_3F ceramics based on the heating temperatures employed. The ε_r was found to initially increase, reaching a maximum value under 750 °C, and then subsequently declined with further rising sintering temperatures. The change in the ε_r and ρ_r values with firing temperature illustrated an analogous variation tendency, suggesting that the ρ_r played a vital role in impacting the ε_r of current ceramics [27]. Moreover, for the samples sintered above 750 °C, the degradation of ε_r was also found to be connected with the disappearance of Li_2TiO_3 (ε_r = 22.0) and the occurrence of LiF (ε_r = 8.0) phases, respectively [17,28].
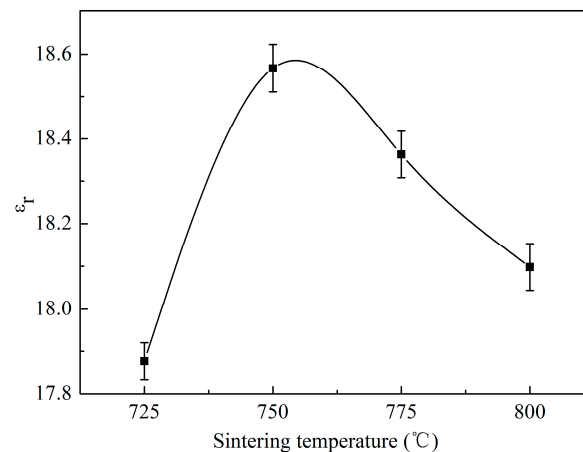
Figure 5. The dependence of the ε_r values of nominal Li_3TiO_3F ceramics on sintering temperature.

The variations of τ_f and $Q \times f$ in nominal Li_3TiO_3F ceramics are illustrated in Figure 6. The τ_f is dependent on phase constitution and crystal structure [8]. In this study, the τ_f exhibited a downward tendency from −42.0 ppm/°C to −48 ppm/°C as the sintering temperature increased from 725 °C, to 800 °C, respectively, which was attributed to the changed phase assemblages (Figure 3) since the LiF registered a negative τ_f (−117.0 ppm/°C), while the Li_2TiO_3 registered a positive τ_f (20.0 ppm/°C) [17,28]. In addition, as the sintering temperature rose from 725 °C, to 750 °C, the $Q \times f$ of Li_3TiO_3F ceramics gradually increased from 52,600 GHz to 57,300 GHz, respectively. Subsequently, the $Q \times f$ values showed a downward trend and ultimately obtained 54,400 GHz at 800 °C. In practical ceramics, the $Q \times f$ is typically dominated by the extrinsic loss rather than intrinsic losses corresponding

to the electromagnetic field interaction with the phonons [29–31]. This extrinsic loss has been associated with microstructural characteristics (such as pores, grain morphology, grain boundaries, and secondary phases, etc.) [32]. The influence of the secondary phases of Li_3TiO_3 ($Q \times f$ = 63,500 GHz) and LiF ($Q \times f$ = 73,800 GHz) on the $Q \times f$ in present ceramics can be ignored due to their relative high $Q \times f$ values [17,28], as shown in Figure 3. Hence the porosity and grain size distribution were considered to determine the $Q \times f$ of present ceramics [32]. The enhancement of $Q \times f$ was associated with the synergistic effects of the enhancement of a uniform microstructure and reduction of porosity, whereas the reduction of $Q \times f$ was associated with the nonuniform and exaggerated grain growth (Figure 2). In addition, the $Q \times f$ value of present ceramics was found to be lower than those of Li_2TiO_3 and LiF, which may be connected with the disordered charge distribution in the crystal as reported in previous research [30,31]. Table 2 summarizes the sintering temperature (T_s) along with the microwave dielectric performances of several rock salt structured ceramics and present ceramics. As shown in Table 2, although the microwave dielectric performances of the present ceramics are somewhat inferior to other counterparts, its remarkable advantages include the relatively low sintering temperature, which is conducive to energy conservation.
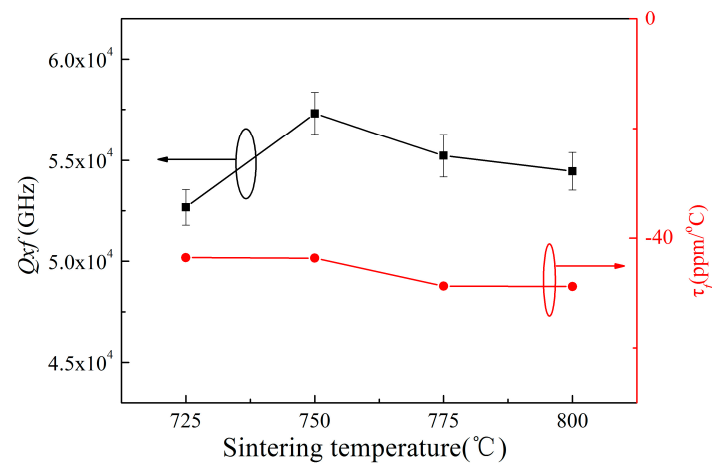
Figure 6. The plots of τ_f and $Q \times f$ in nominal Li_3TiO_3F ceramics with respect to the sintering temperature.

Table 2. The sintering temperature (T_s), along with the microwave dielectric performances of several rock salt structured ceramics and present ceramics.

Compounds	ε_r	Q × f(GHz)	τ_f (ppm/°C)	T_S (°C)	Ref.
$Li_7Ti_3O_9F$	22.5	88 200	−24.0	950	[10]
$Li_5Ti_2O_6F$	19.6	79 500	−30.0	880	[11]
Li_3ZrO_3F	15.8	65 100	1.0	925	[16]
Li_2TiO_3	22.0	63 500	20.0	1300	[17]
Li_3TiO_3F	18.6	30 000	−58.0	875	[20]
Li_3TiO_3F	18.0	57 300	−42.0	750	This study

4. Conclusions

The relationships between the microstructure and microwave dielectric properties of Li_3TiO_3F ceramics were investigated in this study. XRD analysis showed that the major phase of Li_3TiO_3F accompanied with small amounts of Li_2TiO_3 and LiF phases were formed. Dense ceramics with a mean grain size of around 210 nm were obtained from Li_3TiO_3F sintered at 750 °C. As the sintering temperature increased, the ε_r and $Q \times f$ values first increased and then decreased, whereas its τ_f decreased slightly. Typically, the nominal Li_3TiO_3F ceramics fired at 750 °C displayed favorable microwave dielectric properties: ε_r =18.0, $Q \times f$ = 57,300 GHz (under 9.2 GHz), and τ_f =−43.0 ppm/°C, respectively.

References

1.　Li, L.; Yang, S.; Wu, S.Y.; Chen, X.M. Nonlinear variation of resonant frequency with temperature and temperature-dependent τ_f in Al_2O_3-TiO_2 microwave dielectric composites. *Appl. Phys. Lett.* **2021**, *118*, 212902. [CrossRef]

2.　Chu, X.; Jiang, J.; Wang, J.Z.; Wu, Y.C.; Gan, L.; Zhang, T.J. A new high-$Q \times f$ Li_4NbO_4F microwave dielectric ceramic for LTCC applications. *Ceram. Int.* **2021**, *47*, 4344–4351. [CrossRef]

3.　Tian, H.R.; Zheng, J.J.; Liu, L.T.; Wu, H.T.; Kimura, H.; Lu, Y.Z.; Yue, Z.X. Structure characteristics and microwave dielectric properties of $Pr_2(Zr_{1-x}Ti_x)_3(MoO_4)_9$ solid solution ceramic with a stable temperature coefficient. *J. Mater. Sci. Technol.* **2022**, *116*, 121–129. [CrossRef]

4.　Tang, Y.; Li, H.; Li, J.; Fang, W.S.; Yang, Y.; Zhang, Z.Y.; Fang, L. Relationship between rattling Mg^{2+} ions and anomalous microwave dielectric behavior in $Ca_{3-x}Mg_{1+x}LiV_3O_{12}$ ceramics with garnet structure. *J. Eur. Ceram. Soc.* **2021**, *41*, 7697–7702. [CrossRef]

5.　Liu, B.; Sha, K.; Zhou, M.F.; Song, K.X.; Huang, Y.H.; Hu, C.C. Novel low-ε_r MGa_2O_4 (M = Ca, Sr) microwave dielectric ceramics for 5G antenna applications at the Sub-6 GHz band. *J. Eur. Ceram. Soc.* **2021**, *41*, 5170–5175. [CrossRef]

6.　Zhang, Q.; Su, H.; Peng, R.; Huang, F.Y.; Wu, X.H.; Tang, X.L. Effect of phase, chemical bond and vibration characteristics on the microwave dielectric properties of temperature-stable $Zn_{1-x}(Li_{0.5}Bi_{0.5})_xMo_xW_{1-x}O_4$ ceramics. *J. Eur. Ceram. Soc.* **2022**, *42*, 2813–2819. [CrossRef]

7.　Hsu, T.H.; Huang, C.L. Low-loss microwave dielectrics of $Li_{2(1-x)}M_xWO_4$ (M= Mg, Zn; x = 0.01 − 0.09) for ULTCC applications. *Mat. Sci. Semicon. Proc.* **2023**, *158*, 107355. [CrossRef]

8.　Kokkonen, M.; Pálvölgyi, P.S.; Sliz, R.; Jantunen, H.L.; Kordas, K.; Myllymäki, S. An ultralow-loss and lightweight cellulose-coated silica foam for planar fresnel zone plate lens applications in future 6G devices. *IEEE Antennas Wirel. Propag. Lett.* **2023**, *22*, 99–103. [CrossRef]

9.　Dahri, M.H.; Jamaluddin, M.H.; Abbasi, M.I.; Kamarudin, M.R. A review of wideband reflectarray antennas for 5G communication systems. *IEEE Access* **2017**, *5*, 17803–17815. [CrossRef]

10.　Zhang, Z.W.; Fang, L.; Xiang, H.C.; Xu, M.Y.; Tang, Y.; Jantunen, H.; Li, C.C. Structural, infrared reflectivity spectra and microwave dielectric properties of the $Li_7Ti_3O_9F$ ceramic. *Ceram. Int.* **2019**, *45*, 10163–10169. [CrossRef]

11.　Zhang, Z.; Tang, Y.; Xiang, H.C.; Yang, A.; Wang, Y.; Yin, C.Z.; Tian, Y.F.; Fang, L. $Li_5Ti_2O_6F$: A new low-loss oxyfluoride microwave dielectric ceramic for LTCC applications. *J. Mater. Sci. Technol.* **2020**, *55*, 107–115. [CrossRef]

12.　Zhai, S.M.; Liu, P. Microwave dielectric properties of rock-salt structured $Li_7(Nb_{1-x}Ti_x)_2O_{8-x}F$ ($0 \leq x \leq 0.10$) system with low sintering temperature. *Ceram. Int.* **2022**, *48*, 28268–28273. [CrossRef]

13.　Zhai, S.M.; Liu, P.; Zhang, S.S. A novel high-Q oxyfluoride $Li_4Mg_2NbO_6F$ microwave dielectric ceramic with low sintering temperature. *J. Eur. Ceram. Soc.* **2021**, *41*, 4478–4483. [CrossRef]

14.　Zhai, S.M.; Liu, P.; Zhang, S.S. Temperature stable $Li_{5.5}Nb_{1.5}O_6F$-based microwave dielectric ceramics for LTCC applications. *Ceram. Int.* **2022**, *48*, 15951–15958. [CrossRef]

15.　Zhai, S.M.; Liu, P.; Wu, S.H. Low temperature sintered $Li_6MgTiNb_{1-x}V_xO_8F$ microwave dielectric ceramics with high-quality factor. *J. Eur. Ceram. Soc.* **2023**, *43*, 82–87. [CrossRef]

16.　Gao, Y.F.; Jiang, J.; Wang, J.Z.; Gan, L.; Jiang, X.M.; Zhang, T.J. $Li_{2+x}ZrO_3F_x$ ($0 \leq x \leq 1.25$): A new high-$Q \times f$ and temperature-stable microwave dielectric ceramic system for LTCC applications. *J. Am. Ceram. Soc.* **2023**, *106*, 1881–1891. [CrossRef]

17.　Yuan, L.L.; Bian, J.J. Microwave dielectric properties of the lithium containing compounds with rock salt structure. *Ferroelectrics* **2009**, *387*, 123–129. [CrossRef]

18.　Zhang, Y.M.; Huang, Y.W.; Wang, S.Y.; Zhang, Y.C. A novel temperature-stable (1-m)Li_2TiO_3-m$Zn_3Nb_2O_8$ microwave dielectric ceramic. *Funct. Mater. Lett.* **2022**, *15*, 2250006. [CrossRef]

19.　Szymanski, N.J.; Zeng, Y.; Bennett, T.; Patil, S.; Keum, J.K.; Self, E.C.; Bai, J.M.; Cai, Z.J.; Giovine, R.; Ouyang, B.; et al. Understanding the fluorination of disordered rocksalt cathodes through rational exploration of synthesis pathways. *Chem. Mater.* **2022**, *34*, 7015–7028. [CrossRef]

20.　Ding, Y.M.; Bian, J.J. Structural evolution, sintering behavior and microwave dielectric properties of (1 − x)Li_2TiO_3 + xLiF ceramics. *Mater. Res. Bull.* **2013**, *48*, 2776–2781. [CrossRef]

21. Souza, N.D.G.; Paiva, D.V.M.; Mazzetto, S.E.; Silva, M.A.S.; Sombra, A.S.B.; Fechine, P.B.A. Microwave dielectric properties of $Ba_5Li_2W_3O_{15}$ ceramic with excess lithium for dielectric resonator antenna application. *J. Electron. Mater.* **2022**, *51*, 761–768. [CrossRef]

22. Larson, A.C.; VonDreele, R.B. General Structure Analysis System (GSAS); In *Los Alamos National Laboratory Report LAUR 86*; 2004. Available online: https://11bm.xray.aps.anl.gov/documents/GSASManual.pdf (accessed on 15 February 2023).

23. Hakki, B.W.; Coleman, P.D. A dielectric resonator method of measuring inductive capacities in the millimeter range. *IEEE Trans. Microw. Theory Tech.* **1960**, *8*, 402–410. [CrossRef]

24. Courtney, W.E. Analysis and evaluation of a method of measuring the complex permittivity and permeability of microwave insulators. *IEEE Trans. Microw. Theory Tech.* **1970**, *18*, 476–485. [CrossRef]

25. Xing, C.; Li, J.Z.; Wang, J.; Chen, H.L.; Qiao, H.Y.; Yin, X.Q.; Wang, Q.; Qi, Z.M.; Shi, F. Internal relations between crystal structures and intrinsic properties of nonstoichiometric $Ba_{1+x}MoO_4$ ceramics. *Inorg. Chem.* **2018**, *57*, 7121–7128. [CrossRef] [PubMed]

26. Jin, W.; Tan, J.J.; Yan, J.X.; Tao, Y.; Yao, N.N.; Ruan, X.M.; Pei, C.J. Effect of LiF addition on the sinterability, crystal structure and microwave dielectric properties of $Li_3Mg_4NbO_8$ ceramics. *J. Ceram. Process. Res.* **2021**, *22*, 675–678.

27. Song, X.Q.; Yin, C.Z.; Zou, Z.Y.; Yang, J.Q.; Zeng, F.F.; Wu, J.M.; Shi, Y.S.; Lu, W.Z.; Lei, W. Structural evolution and microwave dielectric properties of $CaTiO_3$-$La(Mg_{2/3}Nb_{1/3})O_3$ ceramics. *J. Am. Ceram. Soc.* **2022**, *105*, 7415–7425. [CrossRef]

28. Song, X.Q.; Du, K.; Li, J.; Lan, X.K.; Lu, W.Z.; Wang, X.H.; Lei, W. Low-fired fluoride microwave dielectric ceramics with low dielectric loss. *Ceram. Int.* **2019**, *45*, 279–286. [CrossRef]

29. Qin, J.C.; Liu, Z.F.; Ma, M.S.; Liu, F.; Qi, Z.M.; Li, Y.X. Structure and microwave dielectric properties of gillespite-type $ACuSi_4O_{10}$ (A = Ca, Sr, Ba) ceramics and quantitative prediction of the $Q×f$ value via Machine Learning. *ACS Appl. Mater. Interfaces* **2021**, *13*, 17817–17826. [CrossRef]

30. Schlömann, E. Dielectric Losses in Ionic Crystals with Disordered Charge Distributions. *Phys. Rev.* **1964**, *135*, 412–418. [CrossRef]

31. Tamura, H. Microwave dielectric losses caused by lattice defects. *J. Eur. Ceram. Soc.* **2006**, *26*, 1775–1780. [CrossRef]

32. Valant, M.; Suvorov, D. Microstructural phenomena in low-firing ceramics. *Mater. Chem. Phys.* **2006**, *26*, 1775–1780. [CrossRef]